Earth Syst. Dynam. Discuss., 3, 1–28, 2012
www.earth-syst-dynam-discuss.net/3/1/2012/
doi:10.5194/esdd-3-1-2012

Earth System Dynamics Discussions

Do GCM's predict the climate... or macroweather?

S. Lovejoy[1], **D. Schertzer**[2], **and D. Varon**[1]

[1]Physics, McGill University, 3600 University st., Montreal, Quebec, Canada
[2]CEREVE, Université Paris Est, 6-8, avenue Blaise Pascal, Cité Descartes, 77455 MARNE-LA-VALLEE Cedex, France

Received: 16 October 2012 – Accepted: 30 October 2012 – Published:

Correspondence to: S. Lovejoy (lovejoy@physics.mcgill.ca)

Published by Copernicus Publications on behalf of the European Geosciences Union.

Abstract

We are used to the weather – climate dichotomy, yet the great majority of the spectral variance of atmospheric fields is in the continuous "background" and this defines instead a trichotomy with a "macroweather" regime in the intermediate range ≈ 10 days to 30 yr. In the weather, macroweather and climate regimes, exponents characterize the type of variability over the entire ranges and it is natural to identify them with qualitatively different synergies of nonlinear dynamical mechanisms that repeat scale after scale. Since climate models are essentially meteorological models (although with extra couplings) it is thus important to determine whether they currently model all three regimes. Using Last Millennium simulations from four GCM's, we show that control runs only reproduce macroweather and that runs with various (reconstructed) climate forcings do somewhat better but have overly weak multicentennial variabilities. A possible explanation is that the models lack – or inadequately treat – important slow "climate" processes such as land-ice or deep ocean dynamics.

1 Introduction

The justification for using GCM's to model the climate was succinctly expressed by Bryson (1997): "weather forecasting is usually treated as an *initial value* problem …climatology deals primarily with a *boundary condition* problem and the patterns and climate devolving there from". The main theoretical criticism of this view is that "nonlinear feedbacks (i.e. two way fluxes) between the air, land, and water eliminate an interpretation of the ocean-atmosphere and land-atmosphere interfaces as boundaries…these interfaces become interactive mediums…(that) must therefore necessarily be considered as part of the predictive system" (Pielke, 1998). More generally from a modelling perspective, it seems plausible that the real problem is how to couple "fast" atmospheric processes with a multitude of "slow" climate processes such as land-ice or deep ocean currents. The necessary couplings may simply not be achievable by simply adding more and more "climate forcings" in the form of slowly changing boundary conditions to the fundamentally fast GCM dynamics.

While this debate is important, it needs to be informed by empirical evidence. Before reviewing quantitative analyses, consider Fig. 1 that shows examples of temperatures from weather scales (1 h) and at two lower resolutions (top curves, 20 days and 1 century). Other atmospheric fields (wind, humidity, precipitation, etc.) are qualitatively the same at least up to the limits of instrument data i.e. ≈ 150 yr; see Lovejoy and Schertzer (2012b) and for a review, Lovejoy and Schertzer (2012e). We see that the weather curves "wander" up or down resembling a drunkard's walk so that temperature differences typically increase over larger and larger distances and over longer and longer periods. In contrast, the 20 day resolution curve has a totally different character with upward fluctuations typically being followed by nearly cancelling downward ones. Averages over longer and longer times tend to converge, apparently vindicating the conventional idea that "the climate is what you expect": we anticipate that at decadal or at least centennial scales that averages will be virtually constant with only slow, small amplitude variations. However the century scale curve (top) shows that on the contrary the temperature once again "wanders" in a weather – like manner (quantified in Fig. 2). There are thus three qualitatively different regimes – not two. While the high frequency regime is clearly the weather and the low frequency regime the climate, the new "in between" regime was described as a "spectral plateau", then "low frequency weather" and later dubbed "macroweather" since it is a kind of large scale weather whose statistics are well reproduced by control runs of GCM's (and stochastic cascade models, see below); it is not a small scale climate regime, Lovejoy and Schertzer (2012e). This trichotomy has been confirmed in several composite wide scale range analyses (Lovejoy and Schertzer, 1986; Pelletier, 1998; Huybers and Curry, 2006a; see Table 1, Fig. 2, also Wunsch, 2003) yet the implications have not been widely considered. In this paper we consider the consequences for GCM climate modelling: do GCM's model macroweather, the climate or both?

ESDD
3, 1–28, 2012

2 Fluctuations

Let us quantify the analysis of Fig. 1 using fluctuations rather than the spectra shown in Fig. 2. Consider a regime where the mean temperature fluctuation $<\Delta T>$varies as a function of time scale (Δt) as $<\Delta T>\approx \Delta t^H$ where H is the fluctuation (also called "non-conservation") exponent ("<.>" indicates statistical averaging). When H>0, fluctuations increase with scale, when H<0, they decrease. To see if this explains the "wandering" and "cancelling" in Fig. 1, we must estimate the fluctuations. Although they are usually defined by the absolute difference ΔT between T at time t and at time $t+\Delta t$, this is not sufficient here. Instead we should use the absolute difference of the mean between t and $t+\Delta t/2$ and between $t+\Delta t/2$ and $t+\Delta t$. Technically, this corresponds to defining fluctuations using "Haar" wavelets rather than "poor man's" wavelets. While the latter is adequate for fluctuations increasing with scale (i.e. H>0), mean absolute differences cannot decrease and so when H<0, they do not correctly estimate fluctuations. The Haar fluctuation (which is useful for $-1<H<1$) is particularly easy to understand since (with proper "calibration") in regions where H>0, it can be made very close to the difference fluctuation (the differencing dominates over the averaging) and in regions where H<0, it can be made close to another simple to interpret "tendency fluctuation" (the averaging dominates over the differencing). While other techniques such as Detrended Fluctuation Analysis (Peng et al., 1994; Kantelhardt et al., 2002; Monetti et al., 2003) perform just as well for determining exponents, they have the disadvantage that their fluctuations (which are standard deviations of the residues of polynomial regressions on the running sum of the original series) are not at all easy to interpret (for a summary see Lovejoy and Schertzer, 2012d and for details see Lovejoy and Schertzer, 2012c).

Beyond the first order (mean) statistics, the variation of the fluctuations with scale can be quantified by their qth order statistics, the structure function $S_q(\Delta t)$ is particularly convenient:

$$S_q(\Delta t) = \langle \Delta T(\Delta t)^q \rangle \tag{1}$$

ESDD
3, 1–28, 2012

where "⟨.⟩" indicates ensemble averaging. In a scaling regime, $S_q(\Delta t)$ is a power law; $S_q(\Delta t) \approx \Delta t^{\xi(q)}$, where the exponent $\xi(q) = qH - K(q)$ and $K(q)$ characterizes the scaling intermittency (with $K(1) = 0$) and H is the fluctuation exponent introduced above. In the macroweather regime $K(2)$ is small ($\approx$ 0.01–0.03), so that the RMS variation $S_2(\Delta t)^{1/2}$ (denoted simply $S(\Delta t)$ below) has the exponent $\xi(2)/2 \approx \xi(1) = H$. In the climate regime the intermittency correction is a bit larger (Schmitt et al., 1995) ($\approx$ 0.12) but the error in using this approximation ($\approx$ 0.06) will be neglected.

When $S(\Delta t)$ is estimated for various in situ, reanalysis, multiproxy and paleo temperatures, one obtains Fig. 3 (see also Fig. 4). The key points to note are (a) the three qualitatively different regimes: weather, macroweather and climate with $S(\Delta t)$ respectively increasing, decreasing and increasing again with scale ($H_w>0$, $H_m<0$, $H_c>0$) and with transitions at $\tau_w \approx$ 5–10 days and $\tau_c \approx$ 10–30 yr, (b) the difference between the local and global fluctuations, (c) the amplitude of glacial/interglacial (ice age) transition corresponds to overall ± 3 to ± 5 K variations i.e. $S(\Delta t) \approx 6$, 10 K: the "interglacial window" – rectangle – in Fig. 3. Since these have half periods of 30–50 kyr, to simplify Fig. 4, the corresponding paleotemperature curves are only hinted by dashed lines (see the double headed arrow). In scaling regimes, the power spectrum is $E(\omega) \approx \omega^{-\beta}$ (ω is the frequency) with $\beta = 1+\xi(2) = 1+2H-K(2)$ so that ignoring intermittency (i.e. $K(2) \approx 0$), $H>0$, $H<0$ corresponds to $\beta>1$, $\beta<1$ respectively. Hence for macroweather ($\tau_c > \Delta t > \tau_w$); log-log spectra appear as fairly flat "spectral plateaus" (Lovejoy and Schertzer, 1986) (Fig. 2).

The scaling composites mentioned above agree on the basic scaling picture while proposing somewhat different parameter values and transition scales τ_c (Table 1). Other analyses of macroweather have been carried out using in situ data (Fraedrich and Blender, 2003; Eichner et al., 2003), sea surface temperatures (Monetti et al., 2003) and $\approx$ 1000 yr long Northern Hemisphere reconstructions (Rybski et al., 2006; see also Lennartz and Bunde, 2009; Lanfredi et al., 2009). Similarly, Huybers and Curry (2006b), used NCEP reanalyses and Blender et al. (2006) (see also Franzke, 2010, 2012) analysed the Holocene Greenland paleotemperatures and found comparable results. Finally, multiproxy reconstructions of the Northern Hemisphere (below) yield similar exponents, see Fig. 3 and for more details, see Lovejoy and Schertzer (2012e).

By considering the Fractionally Integrated Flux models (FIF, i.e. cascades (Schertzer and Lovejoy, 1987)) it was argued that whereas in the weather regime, fluctuations depend on interactions in both space and in time, at lower frequencies, only the temporal interactions are important, so that τ_w marks a "dimensional transition". The basic FIF model predicts macroweather exponents to be typically in the range $-0.4<H<-0.3$ (i.e. $0.2<\beta<0.4$) and allows the transition scale τ_w to be estimated theoretically – and essentially from first principles – by first considering the earth's absorbed solar energy and its average rate of conversion into kinetic energy. This yields an estimate close to the empirical tropospheric mean energy flux which is $\varepsilon \approx 10^{-3}\,\mathrm{W\,Kg}^{-1}$ and which implies $\tau_w = \varepsilon^{-1/3} L_e^{2/3} \approx 10$ days (where $L_e = 20\,000$ km is the largest distance on the earth, see Lovejoy and Schertzer, 2010 and Lovejoy and Schertzer, 2012d).

3 The unforced low frequency variability of GCMs (control runs)

Averages over the stable ($H<0$) macroweather regime can be used to define "climate states", and long term changes in these states (in the $H>0$ climate regime) correspond to climate change. The challenge for GCM's is therefore to reproduce the growing fluctuations at time scales $>\tau_c$. In Fig. 4, we show $S(\Delta t)$ from various GCM control runs i.e. with constant orbital and solar parameters, no volcanism, constant Greenhouse gases and fixed land use for both the IPSL model and the more recent Earth Forecasting System (EFS (Jungclaus et al., 2010) see Table 2 for model details). We see that their statistics are the same as those of macroweather all the way to their low frequency limits (see Table 3 for parameters).

Figure 4 also shows $S(\Delta t)$ from the low frequency extension of the stochastic FIF cascade model. These structure functions are compared to the corresponding empirical functions, we can clearly see a strong divergence between the empirical and model

ESDD
3, 1–28, 2012

$S(\Delta t)$ for $\Delta t >\approx 10$–30 yr. With the exception of a spurious "bump" at $\Delta t \approx 2$–4 yr scale in the EFS $S(\Delta t)$, the models do a reasonable job at reproducing the average variability between about one month up to $\tau_c \approx 10$–30 yr. Beyond that however, their mean fluctuations continue to decline whereas the empirical $S(\Delta t)$ starts to rise. The grid scale analyses of the control runs lead us to exactly the same conclusion; indeed the low frequency exponents are all near the same value corresponding to $H \approx -0.4$ ($\beta \approx 0.2$). With the exception of the somewhat larger $S(\Delta t)$ from the EFS model, the GCM and empirical surface $S(\Delta t)$ functions are within $\approx \pm 0.05$ K of each other out to $\Delta t \approx 7$–10 yr. However at longer time scales Fig. 4 shows that the empirical $S(\Delta t)$ closely agree with each other but strongly diverge from the control runs. Whereas the instrumental and multiproxy $S(\Delta t)$ at 100 yr are ≈ 0.6 and ≈ 0.3 K, and rapidly growing, the IPSL and EFS $S(\Delta t)$'s are ≈ 0.1 and 0.2 K and are rapidly decreasing.

These findings are in accord with other studies of the low frequency behaviour of GCM's, including some on "ultra long" (Blender et al., 2006) 10 kyr runs using the Detrended Fluctuation Analysis technique. Note that grid scale statistics have a transition τ_c at slightly longer time scales than the global ones that were analyzed in Fig. 4. The basic conclusions of the studies have been pretty uniform: the low frequency behaviour was scaling, predominantly with $0<\beta<0.6$ (roughly $-0.5<H<-0.3$ i.e. in the same range as our control runs) and with ocean values a little higher than for land (Table 3). The exponents were robust: for example, with a fixed scenario they were insensitive to the use of different models, in the same model, to the addition of greenhouse gases (Fraedrich and Blender, 2003), or in the last 1000 yr in the Northern Hemisphere, to constant or to historically changing drivers (Rybski et al., 2008). Finally, models with sophisticated sea ice rheology also had similar scaling (Fraedrich and Blender, 2003). In no cases and at no geographical location was there evidence of an end to the macroweather regime. Apparently, the global scale IPSL and EFS control run analyses in Fig. 4 are typical.

4 The Last Millenium simulations: the climate or macroweather?

If control runs produce only macroweather, what about forced runs with more realistic low frequency variability? To answer this question, we considered simulations over the last millennium: the ECHO-G "Erik the Red" simulation (von Storch et al., 2004), two EFS simulations (Jungclaus et al., 2010) and eight GISS-E simulations (Schmidt et al., 2006, 2011, 2012). The ECHO-G simulation was chosen because in the IPCC AR4 (Solomon et al., 2007), twelve different Millenium simulations were compared (although only two were full GCM's) and it was noted that ECHO-G had significantly stronger low frequency variability than any of the others. Indeed, Osborn et al. (2006) found that due to initialization problems and lack of sulphates, that ECHO-G was only reliable over the period 1300–1900 AD; our range 1500–1900 AD was free of these problems. The more recent EFS and GISS-E models allow us to explore the impacts of several different forcing and land use reconstructions.

Since the earth's orbital parameters have changed little in the last 1000 yr, if we exclude the 20th century, the key forcings are volcanic and solar. Both EFS and ECHO-G simulations used similar "reconstructed" volcanic forcings; the correct solar reconstructions are much less certain. The amplitudes (i.e. calibration) of the "reconstructed" solar forcings are described in terms of percentages of variation since the 17th century "Maunder minimum". Values of 0.1 % and 0.25 % are considered respectively low and high solar forcing values (see Krivova and Solanki, 2008 for a recent review). In these terms, the ECHO-G forcings were "high" (0.25 %) whereas the EFS simulations were run at both 0.1 % and 0.25 % levels. The GISS-E simulations compared both Steinhilber et al. (2009) and Vieira et al. (2011) solar reconstructions corresponding to smaller (0.06 % and 0.10 %) variations. Only the pre-1610 part of the reconstructions were based on the (statistically quite different) ^{10}Be based reconstructions so that over the analysed range (1500–1900 AD) these percentages capture the main reconstruction differences (see below and Table 4 for a summary).

ESDD
3, 1–28, 2012

In order to determine the natural variability (i.e. without strong anthropogenic effects), we focused on the pre-1900 period. For ECHO-G, EFS, the key conclusions are:

a. The overall EFS variability (Fig. 5) is very close to the corresponding control run (Fig. 4); it is much too weak.

b. The global scale low frequency variability (Fig. 5) of the forced GCM's decrease with increasing Δt and the EFS macroweather behaviour has $S(\Delta t) \approx \Delta t^{-0.4}$.

c. The grid scale (forced) ECHO-G simulation (but not the forced EFS, Fig. 6) has relatively realistic multicentennial variability (close to the post 2003 multiproxies) with roughly the same τ_c and H as the data and the Northern Hemisphere multiproxies.

We found that the forced GISS-E simulations were strongly clustered according to changes in the volcanic forcing used; the highest decadal and multi-decadal variability simulations used the Gao et al. (2008), the weaker ones the Crowley et al. (2008) reconstruction ("Gao", "Crowley" in Fig. 7). Only in the two runs with no volcanic forcing was the impact of different solar forcings detectable. In order to simplify the presentation, we averaged over the three Gao and three Crowley volcanic and the two solar-only runs and compared the results to the mean of the three post 2003 multiproxy reconstructions from Fig. 3. First, we note that at $\approx \tau_c$, the sign of the all the slopes changes. However, the volcanic series vary in the opposite direction from the data: first growing and then decreasing with scale. Only the volcano-free solar forcing runs (Fig. 7, bottom) qualitatively follow the data by first decreasing and then increasing with scale. When compared to the surface series and multiproxies we see that whereas at $\Delta t \approx 10$ yr, the volcanic forcings are factors 2–4 too large, at 400 yr scales they are factors 1.5–4 too small. In contrast the solar forcing is too weak by a roughly constant factor ≈ 1.5 and ≈ 2 at 10 yr and ≈ 400 yr respectively (its climate exponent $H_T \approx 0.1$ is too low when compared with various paleo data exponents which are in the range 0.2–0.4).

These results can be understood with the help of the analyses of Lovejoy and Schertzer (2012a), that showed that whereas the volcanic forcings rapidly become

ESDD
3, 1–28, 2012

smaller at large scales ($H_{vol} \approx -0.4$), that the sunspot based solar reconstructions have $H_{sol} \approx +0.4$ hence grow with scale (Fig. 8). In contrast, the ^{10}Be reconstructions used for the pre 1610 part of the forcing (Vieira et al., 2011) have decreasing fluctuations with $H_{sol} \approx -0.4$. This helps explain the somewhat smaller value $H_T \approx 0.0$ found for the corresponding climate temperature exponent over the earliest 400 yr GISS-E simulation period (850–1250 AD).

5 Conclusions

We reviewed evidence that the variability of the atmosphere out to $\tau_c \approx 10$–30 yr is dominated by weather and macroweather dynamics, that there are neither significant new internal mechanisms of variability nor important new sources of external forcing. τ_c marks a qualitative transition between a higher frequency regime whose fluctuations decrease with scale ($H<0$), and the climate regime where they increase with scale ($H>0$).

We showed that control runs of GCM's (studied in the literature and confirmed here) have overly weak low frequency variability, with no low frequency $H>0$ regime even at scales of millennia. The forced runs were not much different notably with low multi centennial variabilities. With the partial exception of ECHO-G and the solar only GISS-E simulations, they were also qualitatively of the wrong type, decreasing rather than increasing with scale. Presumably, if the climate forcing was of the right type and sufficiently strong, a $H>0$ climate regime would appear. However, in a recent paper Lovejoy and Schertzer (2012a), we examined the scale dependence of fluctuations in the radiative forcings (ΔR_F) of several solar and volcanic reconstructions, finding that they generally were scaling with $\Delta R_F \approx A \Delta t^{H_R}$ (see Table 4 and Fig. 8). If $H_R \approx H_T \approx 0.4$, scale *independent* amplification/feedback mechanisms would suffice. However we often found $H_R \approx -0.3$ implying that the forcings become weaker with scale – even though the response grows with scale. This suggests the need to introduce new slow mechanisms of internal climate variability. Such mechanisms must have broad spectra; this

ESDD
3, 1–28, 2012

suggests their dynamics involve nonlinearly interacting spatial degrees of freedom. Promising candidates include deep ocean currents and land-ice but many other slow climate processes exist.

Acknowledgements. We would like to thank G. Schmidt and R. Pielke Sr. for helpful comments.

References

Blender, R., Fraedrich, K., and Hunt, B.: Millennial climate variability: GCM-simulation and Greenland ice cores, Geophys. Res. Lett., 33, L04710, doi:10.1029/2005GL024919, 2006.

Bryson, R. A.: The Paradigm of Climatology: An Essay, B. Am. Meteorol. Soc., 78, 450–456, 1997.

Crowley, T. J.: Causes of Climate Change Over the Past 1000 Years, Science, 289, 270, doi:10.1126/science.289.5477.270, 2000.

Crowley, T. J., Zielinski, G., Vinther, B., Udisti, R., Kreutzs, K., Cole-Dai, J., and Castellano, E.: Volcanism and the Little Ice Age, PAGES Newslett., 16, 22–23, 2008.

Eichner, J. F., Koscielny-Bunde, E., Bunde, A., Havlin, S., and Schellnhuber, H.-J.: Power-law persistance and trends in the atmosphere: A detailed studey of long temperature records, Phys. Rev. E, 68, 046133–046135, 2003.

Fichefet, T. and Morales Maqueda, M. A.: Sensitivity of a global sea ice model to the treatment of ice thermodynamics and dynamics, J. Geophys. Res., 102, 12609–612646, 1997.

Fraedrich, K. and Blender, K.: Scaling of Atmosphere and Ocean Temperature Correlations in Observations and Climate Models, Phys. Rev. Lett., 90, 108501–108504, 2003.

Fraedrich, K., Blender, R., and Zhu, X.: Continuum Climate Variability: Long-Term Memory, Scaling, and 1/f-Noise, Int. J. Mod. Phys. B, 23, 5403–5416, 2009.

Franzke, C.: Long-range dependence and climate noise characteristics of Antarctica temperature data, J. Climate, 23, 6074–6081, doi:10.1175/2010JCL13654.1, 2010.

Franzke, C.: Nonlinear trends, long-range dependence and climate noise properties of temperature, J. Climate, 25, 4172–4183, doi:10.1175/JCLI-D-11-00293.1, 2012.

Gao, C. G., Robock, A., and Ammann, C.: Volcanic forcing of climate over the past 1500 years: and improved ice core-based index for climate models, J. Geophys. Res., 113, D23111, doi:10.1029/2008JD010239, 2008.

ESDD
3, 1–28, 2012

Do GCM's predict the climate... or macroweather?

S. Lovejoy et al.

Hourdin, F., Musat, I., Bony, S., Braconnot, P., Codron, F., Dufresne, J.-L., Fairhead, L., Filiberti, M.-A., Friedlingstein, P., Grandpeix, J.-Y., Krinner, G., LeVan, P.,, Li, Z.-X., and Lott, F.: The LMDZ4 general circulation model: climate performance and sensitivity to parametrized physics with emphasis on tropical convection, Clim. Dynam., 27, 787–813, doi:10.1007/s00382-006-0158-0, 2006.

Huang, S.: Merging Information from Different Resources for New Insights into Climate Change in the Past and Future, Geophys. Res, Lett., 31, L13205, doi:10.1029/2004GL019781, 2004.

Huybers, P. and Curry, W.: Links between annual, Milankovitch and continuum temperature variability, Nature, 441, 329–332, doi:10.1038/nature04745, 2006a.

Huybers, P. and Curry, W.: Links between annual, Milankovitch, and continuum temperature variability, Nature, 441, 329–332, doi:10.1038/nature04745, 2006b.

Jungclaus, J. H., Keenlyside, N., Botzet, M., Haak, H., Luo, J.-J., Latif, M., Marotzke, J., Mikolajewicz, U., and Roeckner, E.: Ocean Circulation and tropical variability in the coupled model ECHAM5/MPIOM, J. Climate, 19, 3952–3972, 2006.

Jungclaus, J. H., Lorenz, S. J., Timmreck, C., Reick, C. H., Brovkin, V., Six, K., Segschneider, J., Giorgetta, M. A., Crowley, T. J., Pongratz, J., Krivova, N. A., Vieira, L. E., Solanki, S. K., Klocke, D., Botzet, M., Esch, M., Gayler, V., Haak, H., Raddatz, T. J., Roeckner, E., Schnur, R., Widmann, H., Claussen, M., Stevens, B., and Marotzke, J.: Climate and carbon-cycle variability over the last millennium, Clim. Past, 6, 723–737, doi:10.5194/cp-6-723-2010, 2010.

Kantelhardt, J. W., Zscchegner, S. A., Koscielny-Bunde, K., Havlin, S., Bunde, A., and Stanley, H. E.: Multifractal detrended fluctuation analysis of nonstationary time series, Physica A, 316, 87–114, 2002.

Krinner, G., Viovy, N., De Noblet-Ducoudre, N., Ogeé, J., Polcher, J., Friedlingstein, P., Ciais, P., Sitch, S., and Prentice, I. C.: A dynamic global vegetation model for studies of the coupled atmosphere-biosphere system, Global Biogeochem. Cy., 19, Gb1015, doi:10.1029/2003gb002199, 2005.

Krivova, N. A. and Solanki, S. K.: Models of Solar Irradiance Variations: Current Status, J. Astrophys. Astr., 29, 151–158, 2008.

Krivova, N. A., Balmaceda, L., and Solanski, S. K.: Reconstruction of solar total irradiance since 1700 from the surface magnetic field flux, Astron. Astrophys., 467, 335–346, doi:10.1051/0004-6361:20066725, 2007.

Lanfredi, M., Simoniello, T., Cuomo, V., and Macchiato, M.: Discriminating low frequency components from long range persistent fluctuations in daily atmospheric temperature variability, Atmos. Chem. Phys., 9, 4537–4544, doi:10.5194/acp-9-4537-2009, 2009.
Lean, J. L.: Evolution of the Sun's Spectral Irradiance Since the Maunder Minimum, Geophys. Res. Lett., 27, 2425–2428, 2000.
Lennartz, S. and Bunde, A.: Trend evaluation in records with long term memory: Application to global warming, Geophys. Res. Lett., 36, L16706, doi:10.1029/2009GL039516, 2009.
Ljundqvist, F. C.: A new reconstruction of temperature variability in the extra – tropical Northern Hemisphere during the last two millennia, Geogr. Ann. A, 92 A(3), 339–351, doi:10.1111/j.1468-0459.2010.00399.x, 2010.
Lovejoy, S. and Schertzer, D.: Scale invariance in climatological temperatures and the spectral plateau, Ann. Geophys., 4B, 401–410, 1986.
Lovejoy, S. and Schertzer, D.: Towards a new synthesis for atmospheric dynamics: space-time cascades, Atmos. Res., 96, 1–52, doi:10.1016/j.atmosres.2010.01.004, 2010.
Lovejoy, S. and Schertzer, D.: Stochastic and scaling climate sensitivities: solar, volcanic and orbital forcings, Geophys. Res. Lett., 39, L11702, doi:10.1029/2012GL051871, 2012a.
Lovejoy, S. and Schertzer, D.: The climate is not what you expect, B. Am. Meteorol. Soc., in press, 2012b.
Lovejoy, S. and Schertzer, D.: Haar wavelets, fluctuations and structure functions: convenient choices for geophysics, Nonlin. Processes Geophys., 19, 513–527, doi:10.5194/npg-19-513-2012, 2012c.
Lovejoy, S. and Schertzer, D.: Low frequency weather and the emergence of the Climate, in: Extreme Events and Natural Hazards: The Complexity Perspective, edited by: Sharma, A. S., Bunde, A., Baker, D., and Dimri, V. P., 231–254, AGU monographs, 2012d.
Lovejoy, S. and Schertzer, D.: The Weather and Climate: Emergent Laws and Multifractal Cascades, 480 pp., Cambridge University Press, Cambridge, 2012e.
Madec, G., Delecluse, P., Imbard, M., and Lévy, C.: OPA 8.1 Ocean General Circulation Model Reference Manual Rep., 97 pp., Laboratoire d'Océanographie DYnamique et de Climatologie, 1998.
Moberg, A., Sonnechkin, D. M., Holmgren, K., and Datsenko, N. M.: Highly variable Northern Hemisphere temperatures reconstructed from low- and high- resolution proxy data, Nature, 433, 613–617, 2005.

Monetti, R. A., Havlin, S., and Bunde, A.: Long-term persistance in the sea surface temeprature fluctuations, Physica A, 320, 581–589, 2003.
Osborn, T. J., Raper, S. C. B., and Briffa, K. R.: Simulated climate change during the last 1,000 years: comparing the ECHO-G general circulation model with the MAGICC simple climate model, Clim. Dynam., 27, 185–197, doi:10.1007/s00382-006-0129-5, 2006.
Pelletier, J. D.: The power spectral density of atmospheric temperature from scales of 10**-2 to 10**6 yr, EPSL, 158, 157–164, 1998.
Peng, C.-K., Buldyrev, S. V., Havlin, S., Simons, M., Stanley, H. E., and Goldberger, A. L.: Mosaic organisation of DNA nucleotides, Phys. Rev. E, 49, 1685–1689, 1994.
Pielke, R.: Climate prediction as an initial value problem, B. Am. Meteorol. Soc., 79, 2743–2746, 1998.
Raddatz, T. J., Reick, C. H., Knorr, W., Kattge, J., Roeckner, E., Schnur, R., Schnitzler, K. G., Wetzel, P., and Jungclaus, J.: Will the tropical land biosphere dominate the climate-carbon feedback during the twenty-first century?, Clim. Dynam., 29, 565–574, 2007.
Roeckner, E., Arpe, K., Bengtsson, L., Christoph, M., Claussen, M., Dümenil, L., Esch, M., Giorgetta, M., Schlese, U., and Schulzweida, U.: The atmospheric general circulation model ECHAM-4: model description and simulation of present-day climateRep., 90 pp., Max-Planck Institute for Meteorology, Hamburg, Germany, 1996.
Rybski, D., Bunde, A., Havlin, S., and von Storch, H.: Long-term persistance in climate and the detection problem, Geophys. Res. Lett., 33, L06718, doi:10.1029/2005GL025591, 2006.
Rybski, D., Bunde, A., and von Storch, H.: Long-term memory in 1000- year simulated temperature records, J. Geophys. Res., 113, D02106, doi:10.1029/2007JD008568, 2008.
Schertzer, D. and Lovejoy, S.: Physical modeling and Analysis of Rain and Clouds by Anisotropic Scaling of Multiplicative Processes, J. Geophys. Res., 92, 9693–9714, 1987.
Schmidt, G. A., Ruedy, R., Hansen, J. E., Aleinov, I.,Bell, N., Bauer, M.,Bauer, S., Cairns, B., Canuto, V., Cheng, Y., Del Genio, A., Faluvegi, G., Friend, A. D., Hall, T. M., Hu, Y., Kelley, M., Kiang, N. Y., Koch, D., Lacis,c A. A., Lerner, J., Lo, K. K., Miller, R. L., Nazarenko, L., Oinas, V.,Perlwitz, J., Perlwitz, J., Rind, D., Romanou, A., Russell, G. L., Sato, M., Shindell, D. T., Stone, P. H., Sun, S., Tausnev, N., Thresher, D., and Yao, M.-S.: Present day atmospheric simulations using GISS ModelE: Comparison to in-situ, satellite and reanalysis data, J. Climate, 19, 153–192 doi:10.1175/JCLI3612.1, 2006.

ESDD
3, 1–28, 2012

Title Page
Abstract | Introduction
Conclusions | References
Tables | Figures
◀| |▶
◀ ▶
Back | Close
Full Screen / Esc
Printer-friendly Version
Interactive Discussion

Schmidt, G. A., Jungclaus, J. H., Ammann, C. M., Bard, E., Braconnot, P., Crowley, T. J., Delaygue, G., Joos, F., Krivova, N. A., Muscheler, R., Otto-Bliesner, B. L., Pongratz, J., Shindell, D. T., Solanki, S. K., Steinhilber, F., and Vieira, L. E. A.: Climate forcing reconstructions for use in PMIP simulations of the last millennium (v1.0), Geosci. Model Dev., 4, 33–45, doi:10.5194/gmd-4-33-2011, 2011.
Schmidt, G. A., Jungclaus, J. H., Ammann, C. M., Bard, E., Braconnot, P., Crowley, T. J., Delaygue, G., Joos, F., Krivova, N. A., Muscheler, R., Otto-Bliesner, B. L., Pongratz, J., Shindell, D. T., Solanki, S. K., Steinhilber, F., and Vieira, L. E. A.: Climate forcing reconstructions for use in PMIP simulations of the Last Millennium (v1.1), Geosci. Model Dev., 5, 185–191, doi:10.5194/gmd-5-185-2012, 2012.
Schmitt, F., Lovejoy, S., and Schertzer, D.: Multifractal analysis of the Greenland Ice-core project climate data, Geophys. Res. Lett, 22, 1689–1692, 1995.
Shapiro, A. I., Schmutz, W., Rozanov, E., Schoell, M., Haberreiter, M., Shapiro, A. V., and Nyeki, S.: A new approach to long-term reconstruction of the solar irradiance leads to large historical solar forcing, Astron. Astrophys., 529, A67, doi:10.1051/0004-6361/201016173, 2011.
Solomon, S., Qin, D., Manning, M., Chen, Z., Marquis, M., Averyt, K., Tignor, M. M. B., and Miller Jr., H. L. (Eds.): Climate Change 2007 The physical science basis, Contribution of Working Group I to the Fourth Assessment Report of the Intergovernmental Panel on Climate Change, Cambridge University press, Cambridge, 2007.
Steinhilber, F., Beer, J., and Frohlich, C.: Total solar irradiance during the Holocene, Geophys. Res. Lett., 36, L19704, doi:10.1029/2009GL040142, 2009.
Vieira, L. E. A., Solanki, S. K., Krivova, N. A., and Usoskin, I.: Evolution of the solar irradiance during the Holocene, Astron. Astroph., A6, 531, doi:10.1051/0004-6361/201015843, 2011.
von Storch, H., Zorita, E., Jones, J. M., Dimitriev, Y., Gonzalez-Rouco, F., and Tett, S. F. B.: Reconstructing Past Climate from Noisy Data, Science, 306, 679–682, 2004.
Vyushin, D., Zhidkov, I., Havlin, S., Bunde, A., and Brenner, S.: Volcanic forcing improves Atmosphere-Ocean Coupled, Geophy. Res. Lett. , 31, L10206, doi:10.1029/2004GL019499, 2004.
Wang, Y.-M., Lean, J. L., and Sheeley, N. R. J.: Modeling the Sun's magnetic field and irradiance since 1713, Astrophys. J., 625, 522–538, 2005.
Wetzel, P., Maier-Reimer, E., Botzet, M., Jungclaus, J. H., Keenlyside, N., and Latif, M.: Effects of ocean biology on the penetrative radiation on a coupled climate model, J. Climate, 19, 3973–3987, 2006.

ESDD
3, 1–28, 2012

Wolff, J. O., Maier-Reimer, E., and Legutke, S.: The Hamburg Ocean Primitive Equation Model HOPERep., 98 pp., German Climate Computer Center (DKRZ), Hamburg, Germany, 1997.
Wunsch, C.: The spectral energy description of climate change including the 100 ky energy, Clim. Dynam., 20, 353–363, 2003.
Zhu, X., Fraederich, L., and Blender, R.: Variability regimes of simulated Atlantic MOC, Geophys. Res. Lett., 33, L21603, doi:10.1029/2006GL027291, 2006.

ESDD
3, 1–28, 2012

Table 1. Intercomparison of exponents and scales: from macroweather (β_m) and climate (β_c) exponents and transition scales from various instrumental/paleo composite statistical analyses. The large τ_c values in the top two row are from data north of 30° N and are probably anomalously large. Ignoring intermittency, the corresponding fluctuation exponents are $H = (1 - \beta)/2$.

	β_m	β_c	Local τ_c	global τ_c
Lovejoy and Schertzer (1986)	<1 (central England)	1.8 (poles)	≈ 400 yr	≈ 5 yr
Pelletier (1998)	0.5 (continental North America)	1.7 (Antarctica)	≈ 300 yr	–
Huybers and Curry (2006a) (tropical sea surface)	0.56 ± 0.08 (NCEP reanalysis)	1.29 ± 0.13 (several different paleotemperatures)	≈ 100 yr	–
Huybers and Curry (2006a) high latitude continental	0.37 ± 0.05 (NCEP reanalysis)	1.64 ± 0.04 (several different paleotemperatures)	≈ 100 yr	–

ESDD
3, 1–28, 2012

Do GCM's predict the climate... or macroweather?

S. Lovejoy et al.

Title Page
Abstract Introduction
Conclusions References
Tables Figures
◂ ▸
Back Close
Full Screen / Esc
Printer-friendly Version
Interactive Discussion

Table 2. Details of the climate simulations.

Model System	Model components and references	GCM characteristics	Experi-ment	Series length (yr)
ECHO-G von Storch et al. (2004)	ECHAM4 Roeckner et al. (1996), HOPE-G, Wolff et al. (1997)	19 vertical levels, T30, (3.75° resolution)	"Erik the Red", 1000 AD to present, ≈ 0.25 % solar forcing	1000
Earth Forecasting System (EFS) Jungclaus et al. (2010)	ECHAM5 GCM MPIOM ocean model, Jungclaus et al. (2006), carbon cycle module HAMOCC5 Wetzel et al. (2006) land surface scheme JSBACH Raddatz et al. (2007)	19 levels, T31 (3.75° resolution)	Millenium, solar forcing 0.1 %, 0.25 %, 1000 AD to present	1000 with full forcing, 3000 yr control run
IPSL climate system model: IPSL-CM4	LMDZ GCM, Hourdin et al. (2006), ORCA2 Ocean model, Madec et al. (1998), LIM Sea-ice model, Fichefet and Morales Maqueda (1997), ORCHIDEE land-surface model, Krinner et al. (2005)	19 levels, 2.5° × 3.75° grid	Control run: 1910–2410, for IPCC AR4	500 yr
GISS-E	Includes ocean, tracer and sea ice models, incorporates land use changes, Schmidt et al. (2006, 2011, 2012)	20 levels, 2° × 2.5° grid	8 runs varying forcings, land use	1150 yr (850–2000 AD)

ESDD
3, 1–28, 2012

Table 3. Summary of scaling studies of GCM temperatures. All the estimates were made using the DFA method; the spectral exponent β was determined from $\beta = 2\alpha - 1$ where $\alpha = H + 1$ is the conventional DFA exponent (this expression ignores intermittency corrections). Ignoring intermittency (small for these series), we have $H = (\beta - 1)/2$.

Reference	Model	Model characteristics	Series length (yr)	Range of scales in analysis	β_m
Fraedrich and Blender (2003) with IPCC scenario IS92a Greenhouse gas emissions	ECHAM4/OPYC	19 levels, T42 OPYC ocean model includes sea ice with rheology	1000 yr	240 yr	≈ 0 continents, ≈ 0.3 coasts, ≈ 1 for oceans
	HadCM3	19 levels, $2.5^\circ \times 3.75^\circ$	1000 yr	240 yr	Same to within ≈ 0.2
Zhu et al. (2006) (pre-industrial control runs)	GFDL	31 levels, T63	500 yr	500 yr	≈ 1
	ECHAM5/MPIOM	24 levels, $2^\circ \times 2^\circ$ (land), $1^\circ \times 1^\circ$ (ocean)	500 yr	500 yr	≈ 1 mid Atlantic overturning
Blender et al. (2006); Fraedrich et al. (2009)	CSIRO atmosphere-ocean model under present-day conditions	9 levels, R 21 horizontal resolution	10 000 yr simulation	3 kyr	0.2–0.8 depending on location
Vyushin et al. (2004) one control simulation, one with historical drivers	ECHO-G = ECHAM4/ HOPE-G	19 vertical levels, T30	1000 yr simulated temperature records	≈ 200 yr	Land 0.2–0.4, ocean 0.4–0.7

Table 4. An intercomparison of various climate radiative forcings (R_F) discussed in Lovejoy and Schertzer (2012a). The exponents were estimated to the nearest 0.1 and the prefactors A are for the formula $\left\langle (\Delta R_F)^2 \right\rangle^{1/2} = A \Delta t^{\xi(2)/2}$ with Δt expressed in years. Note that Vieira et al. (2011) combined both sunspot and ^{10}Be recontstructions.

Series type	Physical basis	Reference	Series length (yr)	Series resolution (yr)	Scale range analysed (yr)	Prefactor A ($\mathrm{W\,m^{-2}}$)	ξ (2)/2 $\approx H_R^*$
Solar	Sunspot based	Lean (2000)	≈ 400	1	10-400	0.035	0.4
		Wang et al. (2005)		1	10–400	0.0074	0.4
		Krivova et al. (2007)		10	20–400	0.015	0.4
Solar	TIMS Satellite		8.7	6 h	1–8	0.04	0.4
	^{14}Be	Steinhilber et al. (2009)	9300	5 yr smoothed to 40 yr	80–9300	0.4	−0.3
		Shapiro et al. (2011)	9000	1 yr, smoothed to 20 yr	40–9000	3.5	−0.3
Volcanic	Volcanic Indices, ice cores, radiance models	Crowley (2000)	1000	1 yr, smoothed to 30 yr	60–1000	2.0	−0.3
	Ice core sulfates radiance models	Gao et al. (2008)	1500	1 yr smoothed 30 yr	60–1000	2.5	−0.3

* The solar series all have low intermittencies so that $\xi(2)/2 \approx H$ whereas the Crowley (2000) and Gao et al. (2008) volcanic series have high intermittencies so that $H \approx \xi(2)/2 + C_1 \approx -0.2$ where $C_1 \approx 0.16$ is the intermittency correction.

ESDD

3, 1–28, 2012

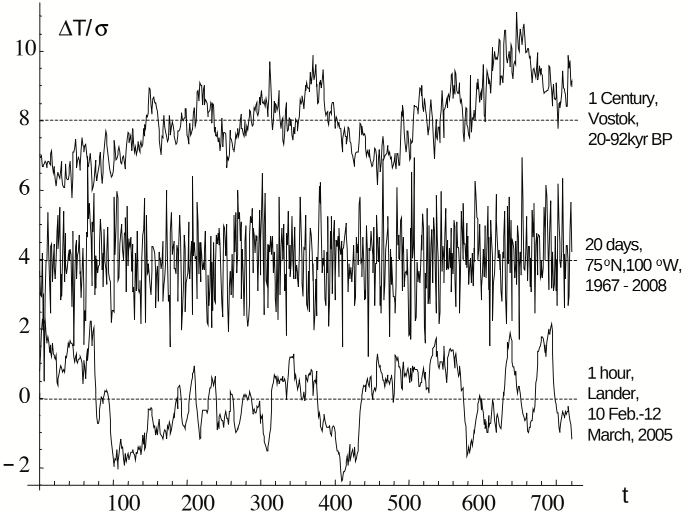

Fig. 1. Dynamics and types of scaling variability: a visual ~~inter~~comparison displaying representative temperature series from weather, macroweather and climate ($H \approx 0.4$, -0.4, 0.4, bottom to top respectively). To make the comparison as fair as possible, in each case, the sample is 720 points long and each series has its mean removed and is normalized by its standard deviation (4.49 K, 2.59 K, 1.39 K, respectively), the two upper series have been displaced in the vertical by four units for clarity. The resolutions are 1 h, 20 days and 1 century respectively, the data are from a weather station in Lander Wyoming, the 20th Century reanalysis and the Vostok Antarctic station respectively. Note the similarity between the type of variability in the weather and climate regimes (reflected in their scaling exponents).

ESDD
3, 1–28, 2012

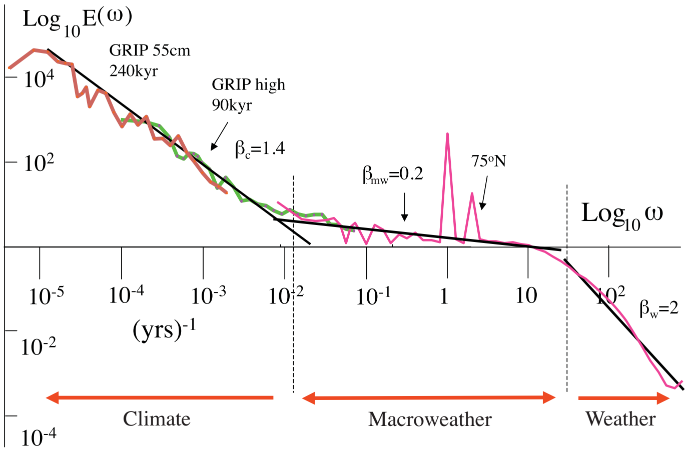

Fig. 2. A composite temperature spectrum: the GRIP (Summit) ice core δ^{18}O a temperature proxy, low resolution (left, brown) along with the first 91 kyr at high resolution (left, green), with the spectrum of the (mean) 75° N 20th Century reanalysis temperature spectrum, at 6 h resolution, from 1871–2008, at 700 mb (right). The overlap (from 10–138 yr scales) is used for calibrating the former (moving them vertically on the log-log plot). All spectra are averaged over logarithmically spaced bins, ten per order of magnitude in frequency. Three regimes are shown corresponding to the weather regime with $\beta_w = 2$ (the diurnal variation and subharmonic at 12 h are visible at the extreme right). The central macro weather "plateau" is shown along with the theoretically predicted $\beta_{mw} = 0.2$–0.4 regime. Finally, at longer time scales (the left), a new scaling climate regime with exponent $\beta_c \approx 1.4$ continues to about 100 kyr. Reproduced from Lovejoy and Schertzer (2012d). The black lines are reference lines with the (absolute) slopes indicated.

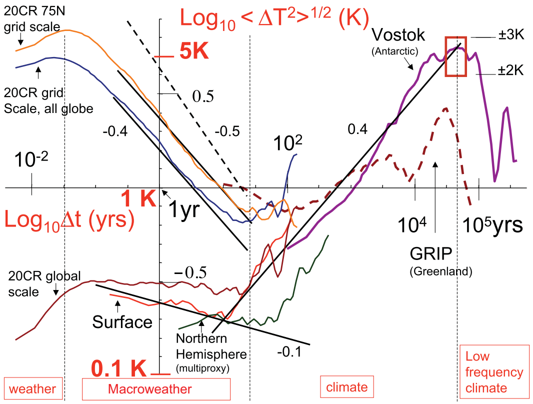

Fig. 3. Empirical RMS temperature fluctuations ($S(\Delta t)$): on the left top we show grid point scale ($2^\circ \times 2^\circ$) daily scale fluctuations for both 75° N and globally averaged along with reference slope $\xi(2)/2 = -0.4 \approx H$ Twentieth Century Reanalysis (20CR), 700 mb. On the lower left, we see at daily resolution, the corresponding globally averaged structure function. Also shown are the averages of the three in situ surface series as well as three post 2003 multiproxy structure functions (1500–1980) described in Lovejoy and Schertzer (2012d), see also Fig. 4. At the right we show both the GRIP (55 cm resolution, with calibration constant 0.5 K mil^{-1}) and the Vostok paleotemperature series. Also shown is the rectangular interglacial "window"; to be consistent with the amplitudes and quasi-periodicity of the glacial/interglacial tansitions (ice ages), the curve must pass through the window. Reproduced from Lovejoy and Schertzer (2012d).

ESDD
3, 1–28, 2012

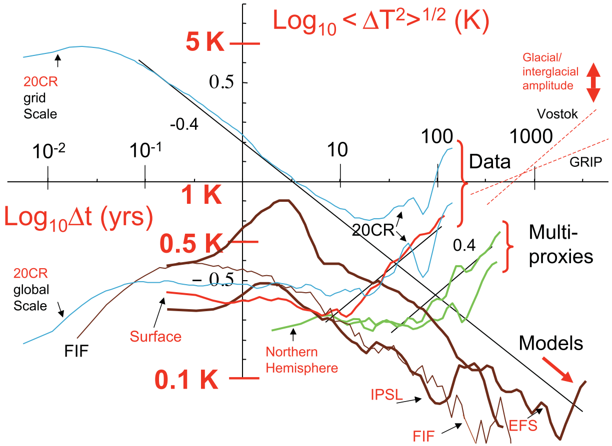

Fig. 4. Control runs versus data: a comparison of the RMS Haar structure functions ($S(\Delta t)$) for temperatures from instrumental (data, daily 20CR, blue; monthly surface series, red), multiproxies (post 2003, yearly resolution, green) GCM control runs (brown thick, monthly) and the FIF stochastic model (brown thin). The data are averaged over hemispheric or global scales (except for the 20CR 2° × 2° grid scale curve which was added for reference). The surface curve is the mean of three surface series (NASA GISS, NOAA CDC and HADCRUT3, all 1881–2008), the 20CR curves are from the 700 mb level, 1871–2008. The multiproxies are means from three post-2003 reconstructions (Huang, 2004; Moberg et al., 2005; Ljundqvist, 2010): two curves are shown, the top from 1500–1980, the bottom from 1500–1900 showing the effect of the 20th century data; see Lovejoy and Schertzer (2012d) for data references and discussion. The y axis values 0.5, −0.5 are the $\log_{10}<\Delta T^2>^{1/2}$ values. The IPSL curve is from a 500 yr control run, the EFS is from a 3000 yr control run; the "bump" at 2–4 yr is a broad quasi periodic model artefact. The reference lines have slopes $\xi(2)/2$ so that $\beta = 1 + \xi(2) = 0.2, 0.4, 1.8$. The amplitude of the Haar structure functions have been calibrated using standard and tendency structure functions and are accurate to within ±25 %. At the upper right we have sketched the Vostok and GRIP paleotemperature $S(\Delta t)$ curves (see Fig. 3) and have indicated the likely glacial/interglacial mean temperature range (difference) by the arrows.

ESDD
3, 1–28, 2012

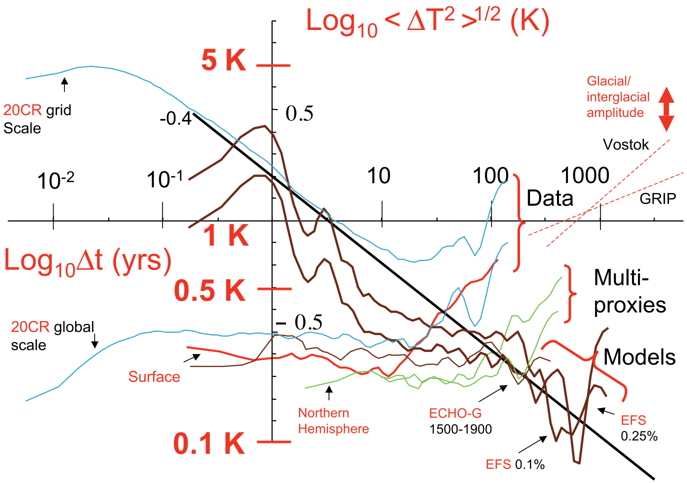

Fig. 5. Forced pre 1900 ~~forced~~ runs versus data, global scale: this is the same as Fig. 4 (global averages) except that the pre 1900 forced ECHO-G (thin brown) and EFS models (thick brown) are analyzed.

ESDD
3, 1–28, 2012

Do GCM's predict the climate... or macroweather?

S. Lovejoy et al.

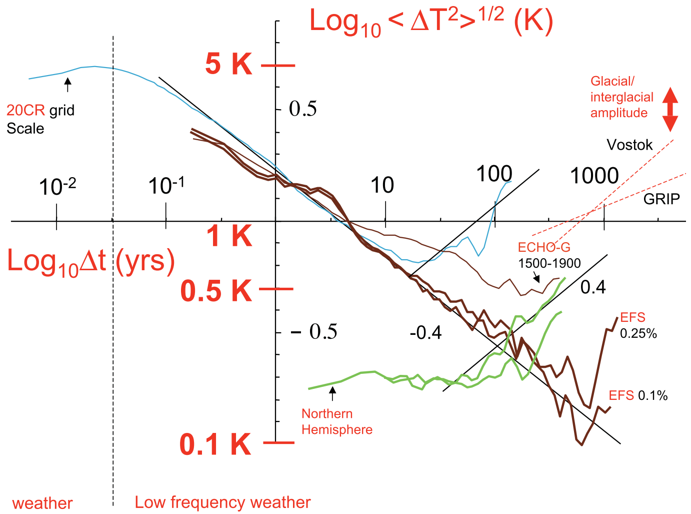

Fig. 6. Grid Scale, forced pre 20th C runs versus data: the same as Fig. 5 except for grid scale analyses (the green Northern Hemisphere multiproxy curves were added for reference, see Fig. 3). Again, the EFS model has low frequencies that are too weak, but even ECHO-G has weak variability and the low frequency tendency is not clear (i.e. is it starting to rise at $\Delta t \approx 500$ yr?).

ESDD
3, 1–28, 2012
Do GCM's predict the climate... or macroweather?
S. Lovejoy et al.

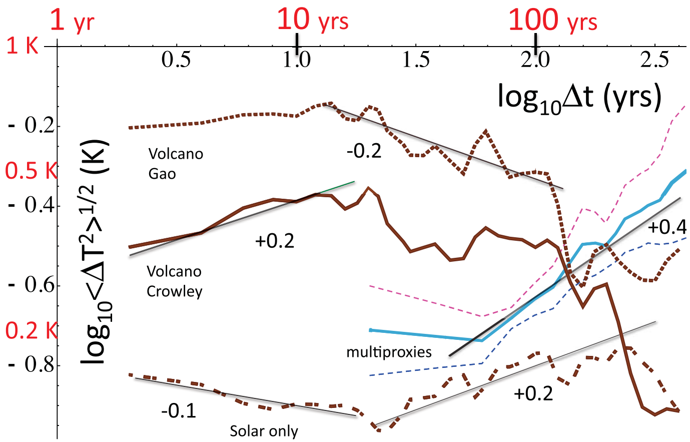

Fig. 7. RMS fluctuations of data and paleo data. Comparison with last millenium simulations for the Northern Hemisphere for 1500–1900, at annual resolution. Gao, Crowley refer to the Gao et al. (2008), and Crowley et al. (2008) solar reconstructions discussed in the text. The multiproxy curves are the means (solid) and one standard deviation limits (dashed) of the post 2003 multiproxies (see Fig. 3) over the period 1500–1900.

ESDD
3, 1–28, 2012

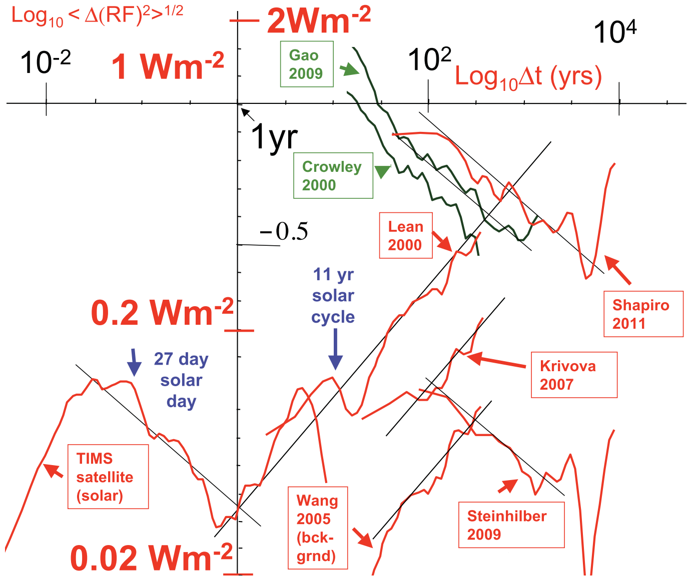

Fig. 8. A comparison of RMS Haar fluctuations for various solar, volcanic, orbital and CO_2 data in units of radiative forcing (R_F). For the solar radiances, the values of estimated Total Solar Insolation were converted into R_F using an albedo = 0.3 and geometric factor 1/4. The TIMS satellite data is for 8.7 yr from 2003 to the present at a 6 h resolution. Note that the Lean (Lean, 2000) reconstruction includes the 11 solar cycle whereas the Wang (Wang et al., 2005) curve is only for the background. The Krivova (Krivova et al., 2007) curve has a 10 yr resolution. The Shapiro (Shapiro et al., 2011) curve (the last 8963 yr) was degraded to 20 yr resolution to average out the solar cycle, the Steinhilber (Steinhilber et al., 2009) curve was at a 40 yr ~~and~~ resolution over the last 9300 yr. The volcanic series were from reconstructions of stratospheric sulphates using ice core proxies. All the structure functions have been increased by a factor of 2 so that they are roughly "calibrated" with the difference (H>0) and tendency (H<0) fluctuations; see Table ~~S~~4. This figure is adapted from Lovejoy and Schertzer (2012a).

ESDD
3, 1–28, 2012